AIP | The Journal of Chemical Physics

Conformer specific dissociation dynamics of iodocyclohexane studied by velocity map imaging

D. K. Zaouris, A. M. Wenge, D. Murdock, T. A. A. Oliver, G. Richmond, G. A. D. Ritchie, R. N. Dixon, and M. N. R. Ashfold

Citation: The Journal of Chemical Physics **135**, 094312 (2011); doi: 10.1063/1.3628682
View online: http://dx.doi.org/10.1063/1.3628682
View Table of Contents: http://scitation.aip.org/content/aip/journal/jcp/135/9?ver=pdfcov
Published by the AIP Publishing

Conformer specific dissociation dynamics of iodocyclohexane studied by velocity map imaging

D. K. Zaouris,[1] A. M. Wenge,[1] D. Murdock,[1] T. A. A. Oliver,[1,a)] G. Richmond,[2] G. A. D. Ritchie,[2] R. N. Dixon,[1] and M. N. R. Ashfold[1,b)]
[1]*School of Chemistry, University of Bristol, Cantock's Close, Bristol BS8 1TS, United Kingdom*
[2]*Department of Chemistry, The Physical and Theoretical Chemistry Laboratory, Oxford University, South Parks Road, Oxford OX1 3QZ, United Kingdom*

(Received 13 July 2011; accepted 5 August 2011; published online 7 September 2011)

The photodissociation dynamics of iodocyclohexane has been studied using velocity map imaging following excitation at many wavelengths within its A-band ($230 \leq \lambda \leq 305$ nm). This molecule exists in two conformations (axial and equatorial), and one aim of the present experiment was to explore the extent to which conformer-specific fragmentation dynamics could be distinguished. Ground (I) and spin-orbit excited (I*) state iodine atom products were monitored by $2 + 1$ resonance enhanced multiphoton ionization, and total kinetic energy release (TKER) spectra and angular distributions derived from analysis of images recorded at all wavelengths studied. TKER spectra obtained at the longer excitation wavelengths show two distinct components, which can be attributed to the two conformers and the different ways in which these partition the excess energy upon C–I bond fission. Companion calculations based on a simple impulsive model suggest that dissociation of the equatorial (axial) conformer preferentially yields vibrationally (rotationally) excited cyclohexyl co-fragments. Both I and I* products are detected at the longest parent absorption wavelength ($\lambda \sim 305$ nm), and both sets of products show recoil anisotropy parameters, $\beta > 1$, implying prompt dissociation following excitation via a transition whose dipole moment is aligned parallel to the C–I bond. The quantum yield for forming I* products, Φ_{I^*}, has been determined by time resolved infrared diode laser absorption methods to be 0.14 ± 0.02 (at $\lambda = 248$ nm) and 0.22 ± 0.05 (at $\lambda = 266$ nm). Electronic structure calculations indicate that the bulk of the A-band absorption is associated with transition to the $4A'$ state, and that the (majority) I atom products arise via non-adiabatic transfer from the $4A'$ potential energy surface (PES) via conical intersection(s) with one or more PESs correlating with ground state products. © *2011 American Institute of Physics*. [doi:10.1063/1.3628682]

I. INTRODUCTION

Organic iodides absorb light in the near ultraviolet (A-band) region, which typically spans the range 200 –300 nm.[1] Photon absorption in this range involves excitation of an electron from a non-bonding p orbital of iodine to an anti-bonding σ^* molecular orbital localised on the C−I bond.[2] $\sigma^* \leftarrow n$ transition results in prompt C−I bond dissociation, producing iodine atoms in their ground ($^2P_{3/2}$) and spin-orbit excited ($^2P_{1/2}$) states (henceforth denoted as I and I*, respectively).

Small iodine containing compounds like hydrogen iodide (HI) (Ref. 3–6) and methyl iodide (CH_3I) (Ref. 7–11) have been investigated extensively and now constitute benchmark systems in the field of photodissociation dynamics. The UV photochemistry of larger alkyl iodides like ethyl,[12] *n*- and *i*-propyl[13] and *n*-butyl iodide[14] has been investigated also (albeit less extensively), iodobenzene[15] (the prototypical aryl iodide) has recently been studied in detail, and three previous studies have addressed aspects of iodocyclohexane (c-$C_6H_{11}I$) photofragmentation at $\lambda = 248$ nm,[16] at ∼304 nm,[17] and at 266 and 277 nm.[18]

Mono-substituted cyclohexanes exist in axial and equatorial conformations, as shown in Fig. 1. In the case of c-$C_6H_{11}I$, spectroscopic studies[19] show the equatorial conformer to be the more stable, by $\Delta G^0 \sim 0.61$ kcal mol^{-1} (∼230 cm^{-1}). This energy difference can be traced primarily to repulsive interactions between the I atom and the H atoms bonded to carbon atoms 3 and 5, which cause the C−I bond in the axial conformer to be slightly weaker and longer.[20,21]

The excited states of c-$C_6H_{11}I$ are best pictured by analogy with CH_3I (in which the I atom is also bonded to a ∼sp^3 hybridised C atom). $\sigma^* \leftarrow n$ excitations in CH_3I give rise to dissociative states labelled (in Mulliken notation[3]) $^3Q_2$, $^3Q_1$, $^3Q_{0-}$, and $^1Q_1$, all of which correlate diabatically with ground state I atoms, and a further set of potentials (including the $^3Q_{0+}$ state) that correlate diabatically to I* products. The A-band of CH_3I is dominated by the $^3Q_{0+} \leftarrow \tilde{X}^1A_1$ absorption (for which the transition dipole moment (TDM) lies parallel to the C−I bond), but weak perpendicular contributions attributable to $^3Q_1 \leftarrow \tilde{X}^1A_1$ and $^1Q_1 \leftarrow \tilde{X}^1A_1$ excitations have been identified at, respectively, long and short wavelengths.[8] *Ab initio* calculations attribute the dominance of the $^3Q_{0+} \leftarrow \tilde{X}^1A_1$ absorption to intensity borrowing from

a)Present address: Department of Chemistry, University of California, Berkeley, California 94720-1460, USA.
b)Author to whom correspondence should be addressed. Electronic mail: mike.ashfold@bris.ac.uk. Tel.: +44 (117) 928 8312. Fax: +44 (117) 925 0612.

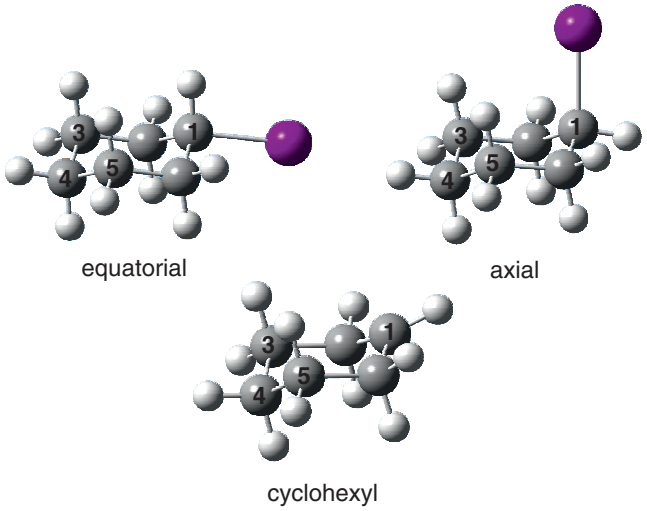

FIG. 1. Minimum energy structures of the equatorial and axial conformers of iodocyclohexane, and of the ground state cyclohexyl radical.

a higher energy $^1A_1$–$\tilde{X}^1A_1$ (C–I bond centred $\sigma^* \leftarrow \sigma$) transition.[11] Iodocyclohexane has lower symmetry (C_S, with the plane defined by the I atom and C atoms 1 and 4), with the result that the degeneracy of the $\Omega \neq 0$ states will be lifted, yielding states of A' and A'' symmetry.

An early laser induced fluorescence study concluded that most of the iodine atom products from 248 nm photolysis of c-$C_6H_{11}I$ were formed in their ground spin-orbit state.[16] Freitas *et al.*[17] investigated c-$C_6H_{11}I$ photolysis at $\lambda \sim 304$ nm by state-selected photofragment translational spectroscopy and identified two sub-groups within the I* atom velocity distribution which they attributed to dissociation of the axial and equatorial conformers; based on the relative intensities of these components, the axial conformer was deduced to yield faster I* + c-C_6H_{11} fragments. More recently, Zhang *et al.*[18] reported a velocity map imaging (VMI) study of c-$C_6H_{11}I$ photolysis at 266 and 277 nm. These authors found that the I and I* products both display near-limiting parallel recoil anisotropy, and concluded that ~70% of the available energy (i.e., the difference between the photon energy and the C−I bond dissociation energy) was partitioned into product internal excitation. They also estimated an I* quantum yield, $\Phi_{I^*} = [I^*]/([I^*] + [I]) > 0.5$ at both wavelengths, but made no reference to possible conformer specific effects in their data analysis.

Here we report a three pronged investigation of the photodissociation dynamics of c-$C_6H_{11}I$ following A-band excitation. VMI has been used to obtain speed (and thus kinetic energy) and angular distributions of the I and I* products resulting from photolysis at many wavelengths in the range 230–305 nm. Time resolved near infrared (IR) absorption measurements on the I* ← I transition at 1.315 μm yield a direct measure of Φ_{I^*} at $\lambda = 248$ and 266 nm. The experimental studies are complemented by spin-orbit resolved *ab initio* calculations of cuts (along R_{C-I}) through the various excited state potential energy surfaces (PESs) correlating to the first two dissociation limits (i.e., to I and I* atoms together with ground state cyclohexyl radicals).

II. EXPERIMENTAL AND DATA ANALYSIS

A. Velocity map imaging studies

1. Experimental setup

The VMI setup used has been described in detail in Ref. 22. Briefly, a mixture of c-$C_6H_{11}I$ (~1.25 mbar; i.e., room temperature vapour pressure[23]) and Ar with a total pressure of ~400 mbar was expanded into the vacuum chamber in the form of a pulsed supersonic beam, collimated by a skimmer and intersected, at right angles, by two counter propagating laser beams. The first laser beam, from a frequency doubled Nd:YAG pumped dye laser (Quanta Ray GCR-170, PDL-2, maximum pulse energy ~1 mJ), was set at many different wavelengths in the range of 230–295 nm and used to dissociate the molecule. The second laser beam (maximum pulse energy ~0.5 mJ), provided by a second frequency doubled Nd:YAG pumped dye laser (Quanta Ray GCR-250, Sirah Cobra Stretch) was tuned to 303.69 and 304.03 nm in order to probe I and I* atoms, respectively, via the well-known 2 + 1 resonance enhanced multiphoton ionization (REMPI) transitions.[24] The time delay between the photolysis and probe laser pulses in the interaction region of the VMI spectrometer was ~20 ns, and the dissociation was carried out in the cold front of the molecular beam. The probe laser wavelength is capable of inducing one photon dissociation of c-$C_6H_{11}I$. Hence, in all two-colour studies, the intensity of this laser was kept as low as possible in order to minimize any one-colour background signal, but the one-colour photolysis (at ~304 nm) was studied in a separate experiment. The bandwidth of the REMPI probe beam is wider than the Doppler profiles of the measured I/I* atoms, so no scanning over the REMPI profile was necessary. All attempts to obtain two-colour images at photolysis wavelengths $\lambda > 305$ nm were unsuccessful. Ions formed in the interaction region were accelerated with a velocity mapping ion optics assembly, through a field free time-of-flight (TOF) region, towards a position sensitive detector (double microchannel plates coupled to a phosphor screen, and a CCD camera). The images were acquired and processed using event counting (LaVision, DaVis 6.2).

2. Image analysis

The fragment distribution $P(v,\theta)$ resulting from a non-saturated one-photon excitation with linearly polarized light can be written as

$$P(v,\theta) = \frac{1}{2} p(v) [1 + \beta(v) P_2(\cos\theta)], \quad (1)$$

where P_2 is the second Legendre polynomial, v is the radial velocity, and θ is the polar angle of the velocity vector with respect to the polarization ($\boldsymbol{\varepsilon}$) vector of the photolysis laser radiation. The distribution function (1) is normalized according to

$$1 = \int_0^{\pi} \sin\theta d\theta \int_0^{\infty} v^2 P(v,\theta) dv. \quad (2)$$

All velocity distributions measured in the present study were modelled as a sum of Gaussian functions, $p_j(v)$, each

with its own value of the anisotropy parameter, β_j.

$$P(v,\theta) = \frac{1}{2}\sum_j p_j(v)\left[1+\beta_j(v)P_2(\cos\theta)\right], \quad (3)$$

with

$$p_j = \frac{A_i}{2\sigma_i}\exp\left(-\frac{1}{2}\left(\frac{v-v_i}{\sigma_i}\right)^2\right), \quad (4)$$

where A_i and σ_i are, respectively, the area and full width half maximum (FWHM) of the Gaussian function.

The measured image is the projection of $P(v,\theta)$, which can be described mathematically by the inverse Abel transform. This transform is numerically stable, but the inversion is a known ill-posed problem. We avoid this difficulty by fitting a projection of Eq. (3) directly to the measured data as described previously.[25] As a check, we also performed the Abel inversion using the matrix method,[26] and confirmed that the total kinetic energy release (TKER) distributions (integrated over θ) returned by the two methods were in good agreement.

The velocity distributions were converted into TKER distributions using the conservation of momentum equation (5).

$$\mathrm{TKER} = \frac{1}{2}m_{\mathrm{I}}\left(1+\frac{m_{\mathrm{I}}}{m_{\mathrm{C_6H_{11}}}}\right)v_{\mathrm{I}}^2. \quad (5)$$

B. I* quantum yield measurements

I* quantum yields, Φ_{I^*}, were measured at $\lambda = 248$ and 266 nm using time-resolved near IR diode laser gain-absorption spectroscopy on the I* ↔ I transition at 1.315 μm.[27] The signal, S_i, recorded immediately after dissociation depends on the population difference between I and I*. At long time, the I* population has decayed to zero; the recorded signal, S_f, is due solely to I atom absorption and depends on the total number of iodine atoms produced in the dissociation process. The quantum yield of I* can be calculated using Eq. (6):[28]

$$\Phi_{\mathrm{I}^*} = \frac{1}{3}\left(1-\frac{S_i}{S_f}\right). \quad (6)$$

Two factors need to be taken into account to ensure that the Φ_{I^*} values returned by this method are reliable. First, addition of molecular O_2 promotes efficient quenching of I* to I, thereby ensuring that all nascent I* atoms have relaxed to the ground spin-orbit state. Second, Ar was added to thermalize the photoproducts translationally, thereby ensuring that the absorption and gain profiles have the same line shape. The present experiments were conducted with both static and flowing samples comprising ~1 mbar c-$C_6H_{11}I$, 1.3 mbar O_2, and 33.3 mbar Ar.

The experimental apparatus has been described previously.[29] The I*($F' = 3$) ↔ I($F'' = 4$) transition is probed with a distributed feedback (DFB) InGaAsP diode laser (Mitsubishi ML776H11F), which is frequency stabilized by locking to a fixed Fabry-Perot etalon via a feedback circuit. The DFB radiation was passed through the reaction cell (length 1.5 m) and narrow band pass filter centred at 1.315 μm and then focused onto a detector (Thorlabs PDA255, 7 ns rise time). The data were collected with a digital oscilloscope, averaging over 30 cycles. The quoted quantum yield values are the result of averaging, typically, 40 such sets of measurements. The 248 and 266 nm radiation was provide by, respectively, a KrF excimer laser (Lambda Physik COMPex 102, output energy ~30 mJ/pulse) and a Nd:YAG laser (Continuum Powerlight 9020, fourth harmonic pulse energy ~50 mJ). The unfocused photolysis and probe beams were co-propagated through the reaction cell, and scattered light from the former was monitored and used as a trigger for data acquisition.

III. QUANTUM CHEMICAL CALCULATIONS

The geometry and harmonic wavenumbers of the axial and equatorial conformers of c-$C_6H_{11}I$ in its ground electronic state and of the ground state of the cyclohexyl radical were calculated at the MP2 level of theory with a 6-311G** basis set,[30,31] using the GAUSSIAN 03 program suite.[32] The calculated (zero-point corrected) energy difference between the two parent conformers is $\Delta E_{\text{ax-eq}} = 227\ \mathrm{cm}^{-1}$ (consistent with the ~230 cm^{-1} value from previous experimental studies[19]), while the calculated barrier to their inter-conversion via a distorted boat-like structure is 2700 cm^{-1} (defined relative to the equatorial conformer). Given a Boltzmann distribution, the relative populations of the two conformers at room temperature is $N_{\mathrm{ax}}/N_{\mathrm{eq}} = 0.33$. The hybridisation of carbon atom 1 changes from ~sp^3 to ~sp^2 upon C–I bond fission; the ∠C2−C1−C6 bond angle changes from ~112° in the ground state molecule to ~118° in the ground state radical.

Based on a state averaged complete active space self consisted field (SA-CASSCF) wavefunction, complete active space with second order perturbation theory and spin-orbit coupling (CASPT2(6/4)) calculations using Dunning's correlation consistent triple ζ basis set[33] and including effective core potentials (ECPs) (Ref. 34) on the iodine atom (cc-pVTZ/cc-pVTZ-PP) have been performed in C_S symmetry using MOLPRO, version 2008.1.[35] To avoid problems due to intruder states in CASPT2 calculations, an imaginary level shift of 0.5 a.u. was necessary. Vertical transition energies were calculated for a range of C–I bond lengths ($R_{\mathrm{C-I}}$). The optimized ground state geometry of the equatorial conformer was used as a reference system, and $R_{\mathrm{C-I}}$ was elongated in a stepwise manner to create a qualitative picture of the spin-orbit free potential energy cuts (PECs) maintaining sp^3 hybridization at the C−I centre. The spin-orbit coupled states were calculated by evaluating $\hat{H}_{SO}$ in a basis of the CASSCF electronic wavefunction but using CASPT2 energies as to allow for some treatment of dynamic correlation. The spin-orbit coupled PECs along $R_{\mathrm{C-I}}$ so derived are shown in Fig. 2(a). In reality, both conformers dissociate to a common cyclohexyl radical [Fig. 1]; the PECs calculated for the axial conformer are indistinguishable on the scale used in Fig. 2(a).

These PECs are reminiscent of those reported previously for HI and CH_3I,[11] although the $\Omega \neq 0$ states are split into (non-degenerate) A' and A'' states as a result of the lowered symmetry. Only for the $4A' \leftarrow \tilde{X}^1A'$ transition (the analogue

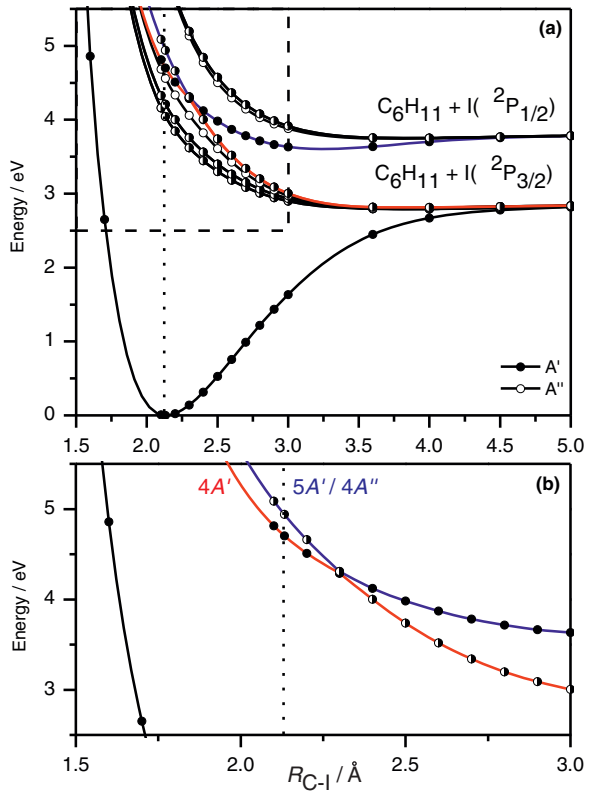

FIG. 2. (a) CASPT2 (6/4) PECs of c-$C_6H_{11}I$ (equatorial conformer) along R_{C-I}. Black (•) and white (○) circles delineate diabatic states of A' and A'' symmetry, respectively, labelled according the C_S point group symmetry. Half-shaded circles indicate A'/A'' pairs that remain essentially degenerate. (b) Selected PECs within the top left hand quadrant of (a), showing the $4A'$ PEC on an expanded scale, and its conical intersection and avoided crossing with, respectively, the $4A''$ and $5A'$ PECs that correlate to the ground state dissociation limit. The dashed vertical line indicates the centre of the vertical Franck-Condon region.

of the $^3Q_{0+} \leftarrow \tilde{X}^1A_1$ transition in CH_3I) does the TDM lie along the C−I bond. Figure 2(b) shows an expanded view of the conical intersection (with the $4A''$ PES) and avoided crossing (with the $5A'$ PES) that are predicted to affect the $4A'$ PES.

IV. EXPERIMENTAL RESULTS

The UV absorption spectrum of a room temperature gas phase sample of c-$C_6H_{11}I$ shown in Fig. 3 serves to highlight the long ($\lambda \sim 305$ nm) and short ($\lambda \sim 230$ nm) wavelength limits of the A-band. Images of I and I* products were recorded across this entire range. All show preferential parallel recoil anisotropy. No I (or I*) images could be obtained at $\lambda \geq 305$ nm.

A. I* images

Figure 4 shows three illustrative I* images, and the corresponding I* product velocity distributions. The images recorded at longer wavelengths appear bimodal—as illustrated by the one-colour image recorded at $\lambda = 304.03$ nm [Fig. 4(a)] and the two-colour I* image obtained at $\lambda = 285$ nm [Fig. 4(b)]. The I* atom velocity distributions

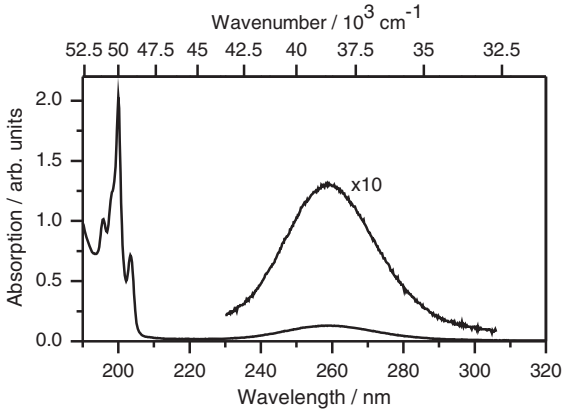

FIG. 3. Ultraviolet absorption spectrum of gas phase iodocyclohexane (room temperature vapour pressure), with the A-band region re-plotted on a 10× expanded vertical scale.

derived from analysis of these images (and those from the other I* (and I) images recorded at longer wavelengths) can be reasonably described using two Gaussian functions, with relative areas ~1:3. Such a ratio lends support to the earlier proposal[17] that the smaller, faster component arises from dissociation of the (less abundant) axial conformer and that the larger, slower feature derives from dissociation of equatorial c-$C_6H_{11}I$ molecules. These velocity sub-groups gradually merge as the photolysis wavelength is reduced—as illustrated for the case of dissociation at $\lambda = 240$ nm [Fig. 4(c)]. The I* (and I) velocity distributions we determine at $\lambda = 275$ and 265 nm are in quantitative accord with those reported in the earlier imaging study,[18] and the deconvolution of the velocity distributions measured at shorter wavelengths becomes more arbitrary. As Fig. 5 shows, the TKER values associated with the means of these velocity components, $TKER_{mean}$, scale near linearly with excitation energy.

Figure 6 shows I* images, the associated TKER distributions (using Eq. (5)), and the β(TKER) values obtained

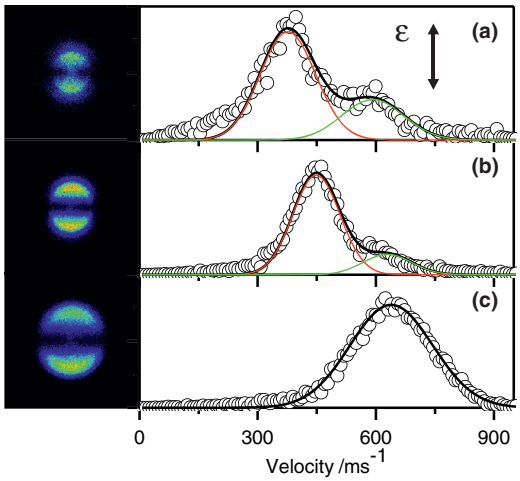

FIG. 4. I* images from photolysis of c-$C_6H_{11}I$ at λ = (a) 304.03 nm, (b) 285 nm, and (c) 240 nm, together with the velocity distributions derived from their analysis and, in (a) and (b), their deconvolution into two Gaussian components. The $\boldsymbol{\varepsilon}$ vector of the photolysis laser beam was aligned vertically in the plane of the detector, as shown by the double-headed black arrow.

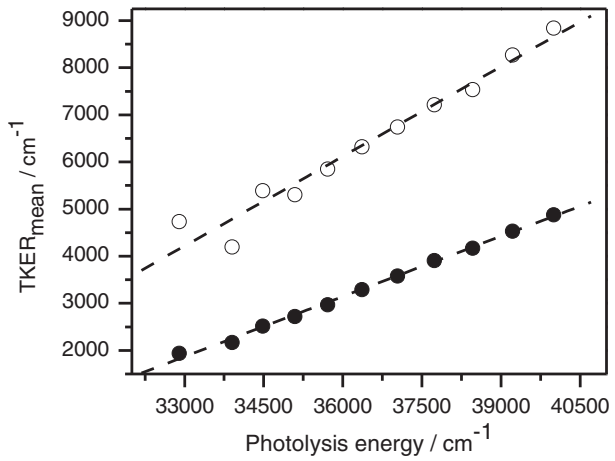

FIG. 5. Variation in $TKER_{mean}$ for the I* products, plotted as a function of excitation energy: (○) fast component, attributed to dissociation of the axial conformer; (●) slower component, attributed to dissociation of the equatorial conformer.

following excitation at the extremes (304.03 nm and 230 nm) and near the centre (265–255 nm) of the A-band. The faster feature in Fig. 6(a), which we attribute to dissociation of the axial conformer, extends to $TKER_{max} \sim 6000\ cm^{-1}$. Given the I*/I spin-orbit splitting, $\Delta E_{SO} = 7603\ cm^{-1}$,[37] and the relative energies of the axial and equatorial conformers of

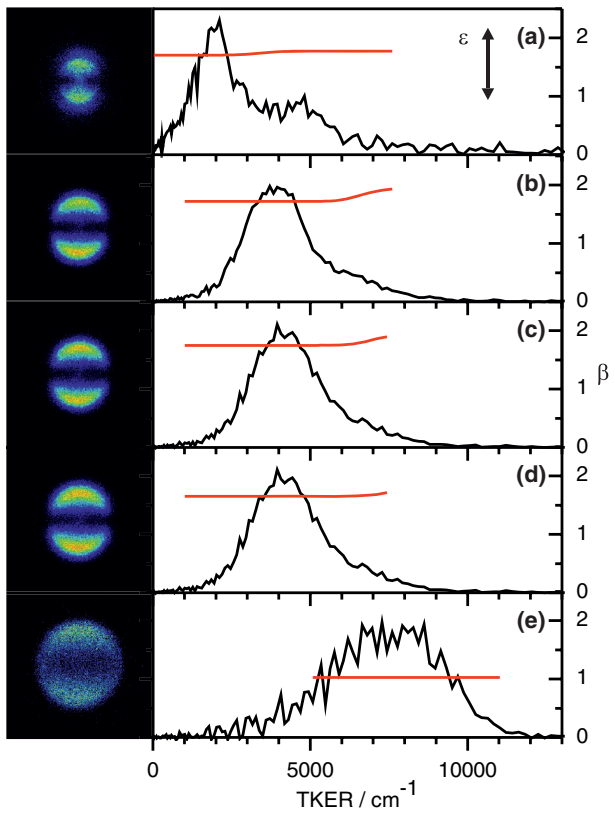

FIG. 6. I* images and the corresponding TKER distributions of the I* + c-C_6H_{11} products from photolysis of c-$C_6H_{11}I$ at λ = (a) 304.03 nm, (b) 265 nm, (c) 260 nm, (d) 255 nm, and (e) 230 nm. The ε vector of the photolysis laser beam was aligned vertically (shown by double-headed black arrow). The red line in each panel shows β, and its variation with TKER derived from the fit approach described in Sec. II A 2.

c-$C_6H_{11}I$, we deduce a value for the C–I bond strength in iodocyclohexane:

$$D_0(\text{I} - \text{cyclohexyl}) \le h\nu + \Delta E_{\text{ax}-\text{eq}} - \Delta E_{SO} - \text{TKER}_{\text{max}} \le 19\,500\ \text{cm}^{-1},$$

in good accord with the value reported by Zhang *et al.*, D_0(I–cyclohexyl) = 229.5 kJ mol^{-1} (19 185 cm^{-1}) (Ref. 18) and sensibly consistent with the C–I bond strength in CH_3I ($D_0(\text{I–CH}_3) = 19\,440 \pm 160\ \text{cm}^{-1}$).[9] The $TKER_{mean}$ values associated with the two features are ∼4900 cm^{-1} and ∼2200 cm^{-1}. Given that the two conformers dissociate to a common radical (plus an I* atom), and that $\Delta E_{\text{ax-eq}}$ is calculated to be only ∼227 cm^{-1}, the large difference in these $TKER_{mean}$ values implies that the cyclohexyl radicals attributed to dissociation of the equatorial conformer at λ = 304.03 nm carry significantly more internal excitation.

Images recorded when exciting near the peak of the A-band, e.g., at λ = 260 nm are less obviously bimodal. Guided by our interpretation of the longer wavelength images, it is tempting to deconvolute such images in terms of a high velocity "tail" extending to $TKER_{max} \sim 8500\ cm^{-1}$ (attributable to dissociation of the axial conformer), and a slower component with $TKER_{mean} \sim 4000\ cm^{-1}$ attributable to dissociation of the equatorial conformer. Given that the available energy (E_{avl}, i.e., the difference between the photon energy and the second dissociation limit) at λ = 260 nm is ∼11 700 cm^{-1}, this $TKER_{mean}$ value implies that ∼65% of E_{avl} is partitioned into internal excitation of the cyclohexyl product. Such trends persist to shorter wavelengths [e.g., Fig. 6(e)], λ = 230 nm), where we find $TKER_{max} \sim 12\,000\ cm^{-1}$ and $TKER_{mean} \sim 7500\ cm^{-1}$ – implying, again, preferential partitioning of the available energy into internal excitation of the radical.

The recoil anisotropy parameter of the I* fragments, and its TKER dependence, has been determined at all wavelengths studied. As Fig. 6 shows, β is positive throughout, close to +2 at the longer wavelengths (especially at higher TKER values), but is clearly smaller (∼+1) at λ = 230 nm. The present results are generally consistent with the earlier findings of Freitas *et al.*[17] who reported (albeit smaller) positive values for β(I*) at λ = 304.02 nm, and with those of Zhang *et al.*[18] who determined β(I*) ∼ 1.8 at λ = 277 nm and ∼1.7 at λ = 266 nm.

B. I images

Images of I atom products formed by photolysis of c-$C_6H_{11}I$ at the extremes (λ = 303.69 nm and 230 nm) and near the centre (λ = 265, 260, and 255 nm) of the A-band of c-$C_6H_{11}I$ are shown in Fig. 7. As with the I* fragments, all of the I products observed at all excitation wavelengths display preferential parallel recoil anisotropy. Again, as with the I* products, the I atoms formed at the longest excitation wavelength (λ = 303.69 nm) display a bimodal TKER distribution, peaking at $TKER_{mean}$ ∼7800 cm^{-1} and ∼5500 cm^{-1}. These contributions progressively merge as the excitation wavelength is reduced, forming a single broad distribution peaking at $TKER_{mean}$ ∼7300 cm^{-1} (at λ = 260 nm) and ∼9300 cm^{-1} (at λ = 230 nm). These $TKER_{mean}$ val-

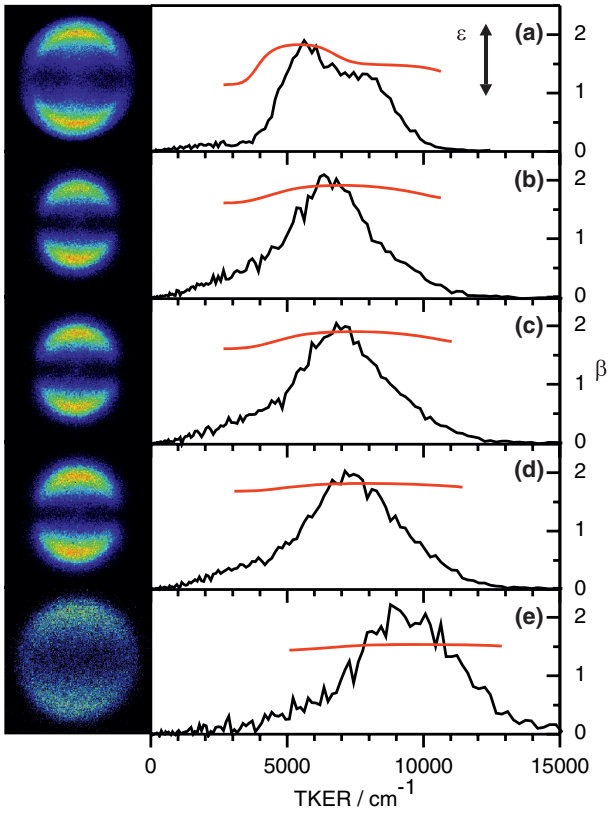

FIG. 7. I images and the corresponding TKER distributions of the I + c-C_6H_{11} products from photolysis of c-$C_6H_{11}I$ at λ = (a) 303.69 nm, (b) 265 nm, (c) 260 nm, (d) 255 nm, and (e) 230 nm. The $\boldsymbol{\varepsilon}$ vector of the photolysis laser beam was aligned vertically (shown by double-headed black arrow). The red line in each panel shows β, and its variation with TKER derived from the fit approach described in Sec. II A 2.

ues represent ∼50% of E_{avl} for this product channel at λ = 303.69 nm, and ∼38% of E_{avl} at λ = 260 nm and 230 nm, again implying efficient channelling of the available energy into internal excitation of the cyclohexyl partner.

C. I* quantum yields

Figure 8 depicts the transient absorption signals measured on the I* ↔ I transition at 1.315 μm following c-$C_6H_{11}I$ photolysis at λ = 248 and 266 nm, and the fits used to establish the initial (S_i) and final (S_f) signals. Quenching by O_2 is the dominant I* loss process under the present experimental conditions, so the observed signal can be described simply by a first order exponential decay. The measured signals are also sensitive to iodine atom diffusion out of the probe beam, which manifests itself as a positive gradient at longer times (t > 50 μs) but makes negligible contribution on the timescales relevant to Fig. 8. The present quantum yield measurements were validated by determining Φ_{I^*} for CH_3I photolysis at λ = 248 nm. The value so determined (0.70 ± 0.03) is in excellent agreement with that reported previously by van Veen *et al.*[36] (0.71 ± 0.02), but a little lower than that reported by Pence *et al.*[38] (0.81 ± 0.03). For c-$C_6H_{11}I$, the Φ_{I^*} values returned at λ = 248 and 266 nm are, respectively, 0.14 ± 0.02 and 0.22 ± 0.05. The error quoted for each of the present Φ_{I^*} measurements is the 2σ value from 40 individual measurements. As Table I shows, the former value is lower than the early estimate by Godwin *et al.*,[16] while the 266 nm value we determine is much lower than that reported by Zhang *et al.*[18] As Haugen *et al.*[27] note, there is a unique reference point in initial gain versus absorption "titration" measurements of the type presented here, at which the initial prompt amplitude vanishes. This occurs at $\Phi_{I^*} = 0.33$ for systems like c-$C_6H_{11}I$ that yield one iodine atom, so the observed prompt drop in signal at $t = 0$ [Fig. 8] immediately points to the fact that Φ_{I^*} must be <0.33 at both λ = 248 and 266 nm.

TABLE I. Φ_{I^*} values determined for c-$C_6H_{11}I$ (and CH_3I) photolysis, in the present work and in previous studies.

	$C_6H_{11}I$		CH_3I	
λ (nm)	Present work	Previous studies	Present work	Previous studies
248	0.14 ± 0.02	0.27 (Ref. 16)	0.70 ± 0.03	0.71 ± 0.02 (Ref. 36) 0.81 ± 0.03 (Ref. 38)
266	0.22 ± 0.05	0.52 (Ref. 18)		

V. DISCUSSION

The I and I* products formed from photolysis of c-$C_6H_{11}I$ at all but the very shortest wavelengths within the A-band display β values approaching +2. This implies that the A-band absorption is dominated by excitation to the $4A'$ state (i.e., the analogue of the $^3Q_{0+} \leftarrow \tilde{X}^1A_1$ absorption in CH_3I), since this is the only excitation for which the TDM lies parallel to the C–I bond. By analogy with CH_3I,[39] the dominance of this parallel absorption may well indicate some intensity stealing from the higher energy $\sigma^* \leftarrow \sigma$ transition. The $4A'$ state of c-$C_6H_{11}I$ correlates diabatically with I* products [Fig. 2], but the recoil anisotropy parameters observed for the (majority) I atom products imply that these must also

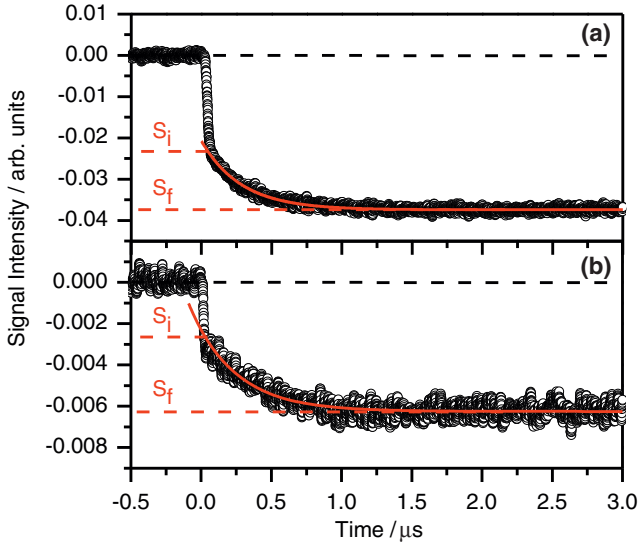

FIG. 8. Time resolved absorption traces (black curves) measured following photolysis of c-$C_6H_{11}I$ at (a) 248 and (b) 266 nm, with the initial (S_i) and final (S_f) signals indicated. The red lines show the exponential fits to these decays.

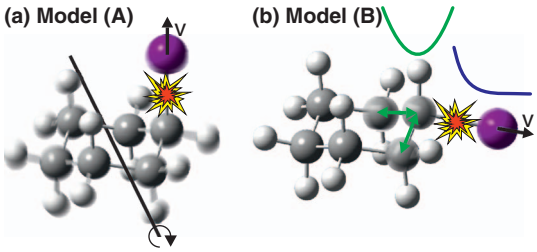

FIG. 9. Schematic illustrations of Models (A) and (B) used to describe sources of internal excitation in the cyclohexyl radical products arising in the near UV photolysis of axial and equatorial conformers of c-$C_6H_{11}I$.

arise via initial $4A' \leftarrow \tilde{X}^1A'$ excitation, with subsequent non-adiabatic coupling to one or more states that correlate to the lowest dissociation limit. Further, given the low Φ_{I^*} values measured, these couplings must be efficient. The C–I bond strength in c-$C_6H_{11}I$ corresponds to an excitation wavelength of ~500 nm. The A-band absorption profile [Fig. 3], and our inability to detect any I atom products following excitation at $\lambda > 305$ nm, both demonstrate that the oscillator strengths to the various repulsive PESs that are calculated to lie below that of the $4A'$ state [Fig. 2] must be very low.

In what follows, we discuss two limiting models of c-$C_6H_{11}I$ photolysis. Neither is wholly realistic, but both may provide some rationale for the observed energy disposals. Model (A) treats the c-C_6H_{11} fragment as a rigid entity, and provides some insight into the recoil anisotropy of the iodine atom products and the likely rotational excitation of the c-C_6H_{11} partner. The electric vector $\boldsymbol{\varepsilon}$ determines the most probable orientation of the photo-excited molecule and, specifically, the C–I bond. Prompt dissociation will involve impulsive separation between the I atom and carbon atom 1. In the molecular frame, the I atom will recoil along an axis close to that defined by the bond—yielding $\beta \sim +2$—and the impulse will exert a torque on the c-C_6H_{11} fragment, generating rotational angular momentum about its b-inertial axis as illustrated in Fig. 9(a). Viewed in terms of an impact parameter model, we can equate

$$\hbar\sqrt{J(J+1)} = \mu_r v b, \tag{7}$$

where μ_r is the reduced mass (8.335×10^{-26} kg), v is the relative velocity of the recoiling fragments, and b is the impact parameter. Consider the specific case of dissociation at $\lambda = 304.03$ nm, yielding I* products. From Figs. 5(a) and 6(a), we estimated $\text{TKER}_{\text{mean}} \sim 4900\ \text{cm}^{-1}$ for the products from dissociation of the axial conformer, implying $v \sim 1510\ \text{m s}^{-1}$. Given D_0(I–cyclohexyl) = 19 185 cm^{-1} and $\Delta E_{\text{ax-eq}} = 227\ \text{cm}^{-1}$, we can estimate the internal (rotational) energy as $E_{\text{rot}} \sim 1100\ \text{cm}^{-1}$. Setting

$$E_{\text{rot}} \approx B\left\langle J_b^2 \right\rangle, \tag{8}$$

and using the calculated value $B \sim 0.151\ \text{cm}^{-1}$, yields $\langle J_b \rangle \sim 85$ and, via Eq. (7) with $J \equiv J_b$, a physically plausible value of b ~0.72 Å. Such a model predicts that E_{rot} should scale linearly with E_{avl}—as observed (recall Fig. 5).

Recalling Fig. 1, the impact parameter b for the analogous C–I bond fission in the equatorial conformer will be smaller, so we must seek an alternative explanation for the deduced higher E_{int} in fragments resulting from this dissociation.

Model (B) recognises that the c-C_6H_{11} fragment is not a rigid entity, and treats the c-$C_6H_{11}I$ molecule as a three component system comprising (A) the I atom, (B) the adjacent CH group, and (C) the remainder of the ring, with respective masses 127, 13, and 70 u. At $t = 0$, E_{avl} is all potential (V_{AB}) and all nuclei are at rest. The initial effect of the impulse arising from C–I bond fission within this Heavy-Light-Heavy system is to drive B into C, thereby exciting a superposition of vibrational modes within the cyclohexyl ring. The fraction of the available energy that remains in the radical product will depend on the extent of vibrational rebound towards A within the dissociation lifetime. Simulations using Model (B) assume an exponential repulsion between A and B, and treat the vibration of B against the rest of the ring using a one-dimensional harmonic potential, as illustrated in Fig. 9(b). The latter is a major approximation: the C_5H_{10} entity contains 39 vibrational degrees of freedom (the c-C_6H_{11} radical has 45), including low frequency bending modes that are likely to be very efficient energy sinks. Nonetheless, Model (B) can reproduce the deduced energy disposal in the c-C_6H_{11} + I* products from 304.03 nm photolysis of the equatorial conformer (i.e., $E_{\text{avl}} = 6100\ \text{cm}^{-1}$, $\text{TKER}_{\text{mean}} \sim 2200\ \text{cm}^{-1}$, $\langle E_{\text{int}} \rangle \sim 3900\ \text{cm}^{-1}$, which is here viewed as product vibration (E_{vib})). Assuming $\alpha \sim 3\ \text{Å}^{-1}$ in the exponential (broadly consistent with the gradient of the *ab initio* $4A'$ potential in the vertical Franck-Condon region [Fig. 2] and f ~7000 cm^{-1} Å^{-2} (giving a representative vibrational frequency ~100 cm^{-1}), dissociation is over in ~30 fs and E_{vib} settles at ~50% of E_{avl}. With such parameters, model (B) predicts that E_{vib} will scale more than linearly with increasing $E_{\text{avl.}}$

Clearly, neither Models (A) nor (B) will provide a quantitative description of the energy disposal in the fragmentation of either conformer, but they do serve to highlight reasons why c-$C_6H_{11}I$ (and other substituted cyclohexanes) should be expected to show conformer specific fragmentation dynamics. Any full picture of the energy disposal in the c-C_6H_{11} fragments formed in partnership with the I* products must recognise both vibrational and rotational contributions arising from the impulsive energy release, plus possible Franck-Condon induced vibrational excitation of the ring as the hybridisation of carbon atom 1 relaxes from ~sp^3 to ~sp^2. Describing the energy disposal in the c-C_6H_{11} fragments formed together with ground state I atoms is likely to be complicated further, by the involvement of (as yet unknown) nuclear motions that facilitate non-adiabatic coupling from the initially populated $4A'$ potential.

VI. CONCLUSIONS

Velocity map imaging studies of the I and I* products resulting from photolysis of iodocyclohexane at many different wavelengths within its A-band absorption ($230 \leq \lambda \leq 305$ nm) support previous suggestions[17] that the energy disposal in the cyclohexyl products is conformer specific. Impulsive model arguments provide a qualitative explanation for the deduced preferential partitioning into product

internal (vibrational) excitation in the case of the equatorial parent conformer. The I and I* products formed at all excitation wavelengths studied display near-limiting parallel recoil anisotropy. This observation is rationalised by spin-orbit resolved electronic structure calculations which associate A-band absorption with excitation to the $4A'$ state (the analogue of the $^3Q_{0+}$ state in HI or CH_3I). Time-resolved IR absorption measurements of the I* ↔ I transition at 1.315 μm following photolysis at $\lambda = 248$ and 266 nm return respective I* quantum yields, Φ_{I^*}, of 0.14 ± 0.02 and 0.22 ± 0.05, highlighting the comparative efficiency of non-adiabatic transfer from the $4A'$ PES to one or more PESs correlating with ground state products. The present results for iodocyclohexane should be contrasted with the results of our recent photofragmentation studies of the cyclic amines morpholine[40] and 3-pyrroline.[41] Both of the latter exist as axial and equatorial conformers, and both undergo prompt N–H bond fission following UV excitation. Kinetic energy measurements of the resulting H atoms allowed resolution of velocity subgroups originating from each conformer, but in neither case did we discern any conformer-specific differences in the pattern of energy disposal within the resulting radical partner—consistent with the minimal impulse caused by loss of the light H atom.

ACKNOWLEDGMENTS

The authors gratefully acknowledge financial support from the Marie Curie Initial Training Network ICONIC (Contract Agreement No. 238671) and EPSRC for the award of a programme grant (EP/G00224X).

[1] D. Perret and C. F. Goodeve, Proc. R. Soc. London, Ser. A **165**, 31 (1938).
[2] K. Kimura and S. Nagakura, Spectrochim. Acta **17**, 166 (1960).
[3] R. S. Mulliken, J. Chem. Phys. **8**, 382 (1940).
[4] S. R. Langford, P. M. Regan, A. J. Orr-Ewing, and M. N. R. Ashfold, Chem. Phys. **231**, 245 (1998).
[5] P. M. Regan, D. Ascenzi, C. Clementi, M. N. R. Ashfold, and A. J. Orr-Ewing, Chem. Phys. Lett. **315**, 187 (1999).
[6] P. M. Regan, D. Ascenzi, E. Wrede, P. A. Cook, M. N. R. Ashfold, and A. J. Orr-Ewing, Phys. Chem. Chem. Phys. **2**, 5364 (2000).
[7] D. W. Chandler and P. L. Houston, J. Chem. Phys. **87**, 1445 (1987).
[8] A. T. J. B. Eppink and D. H. Parker, J. Chem. Phys. **109**, 4758 (1998).
[9] A. T. J. B. Eppink and D. H. Parker, J. Chem. Phys. **110**, 832 (1999).
[10] F. Aguirre and S. T. Pratt, J. Chem. Phys. **122**, 234303 (2005).
[11] A. B. Alekseyev, H.-P. Liebermann, R. J. Buenker, and S. N. Yurchenko, J. Chem. Phys. **126**, 234102 (2007).
[12] Y. Tang, W.-B. Lee, Z. Hu, B. Zhang, and K.-C. Lin, J. Chem. Phys. **126**, 064302 (2007).
[13] H. Fan and T. Pratt, J. Chem. Phys. **123**, 204301 (2005).
[14] W. K. Kang, K. W. Jun, K.-H. Jung, and H. J. Hwang, J. Phys. Chem. **98**, 1525 (1994).
[15] A. G. Sage, T. A. A. Oliver, D. Murdock, M. B. Crow, G. A. D. Ritchie, J. N. Harvey, and M. N. R. Ashfold, Phys. Chem. Chem. Phys. **13**, 8075 (2011).
[16] F. G. Godwin, P. A. Gorry, P. M. Hughes, D. Raybone, T. M. Watkinson, and J. C. Whitehead, Chem. Phys. Lett. **135**, 163 (1987).
[17] J. E. Freitas, H. J. Hwang, A. B. Ticknor, and M. A. El-Sayed, Chem. Phys. Lett. **183**, 165 (1991).
[18] R. Zhang, A. Y. Ghazai, Y. Liu, Y. Zhang, B. Tang, and B. Zhang, Opt. Commun. **282**, 2169 (2009).
[19] D. E. Bugay, C. H. Bushweller, C. T. Danehey, Jr., S. Hoogasian, J. A. Blersch, and W. R. Leenstra, J. Phys. Chem. **93**, 3908 (1989).
[20] A. Y. Meyer, J. Mol. Struct.: THEOCHEM **94**, 95 (1983).
[21] D. Damiani, F. Scappini, W. Caminati, and G. Corbelli, J. Mol. Spectrosc. **100**, 36 (1983).
[22] E. Wrede, S. Laubach, S. Schulenburg, A. Brown, E. R. wouters, A. J. Orr-Ewing, and M. N. R. Ashfold, J. Chem. Phys. **114**, 2629 (2001).
[23] M. Fulem, K. Růžička, P. Morávek, J. Pangrác, E. Hulicius, B. Kozyrkin, and V. Shatunov, J. Chem. Eng. Data **55**, 4780 (2010).
[24] L. Minnhagen, Ark. Fys. **21**, 415 (1962).
[25] A. M. Wenge, U. Kensy, and B. Dick, Phys. Chem. Chem. Phys. **12**, 4644 (2010).
[26] G. Pretzler, H. Jäger, T. Neger, H. Philipp, and J. Woisetschläger, Z. Naturforsch. **47a**, 955 (1992).
[27] H. K. Haugen, E. Weitz, and S. R. Leone, J. Chem. Phys. **83**, 3402 (1985).
[28] Haugen *et al.* (Ref. 27) define the relationship between S_i, S_f, and Φ_{I^*} as: $\Phi_{I^*} = 1/3(S_i/S_f + 1)$ and implicitly assume that the modulus of the experimentally measured S_f value is used when calculating Φ_{I^*} [W. P. Hess and S. R. Leone, J. Chem. Phys. **86**, 3773 (1987)]. The present Eq. (6), in contrast, employs the absolute measured S_f value. The difference between the two expressions for Φ_{I^*} can be understood as follows: Haugen *et al.* define I absorption as a negative contribution to S_i (with stimulated emission from I* giving a positive contribution), while treating absorption as a positive quantity in the case of S_f (see Eq. 2 of Ref. 27). We find it more satisfactory to define absorption as having a consistent sign throughout.
[29] A. Gilchrist, G. Hancock, R. Peverall, G. Richmond, G. A. D. Ritchie, and S. Taylor, J. Phys. Chem. A **112**, 4531 (2008).
[30] R. Krishnan, J. S. Binkley, R. Seeger, and J. A. Pople, J. Chem. Phys. **72**, 650 (1980).
[31] M. N. Glukhovtsev, A. Pross, M. P. McGrath, and L. Radom, J. Chem. Phys. **103**, 1878 (1995).
[32] M. J. Frisch, G. W. Trucks, H. B. Schlegel, G. E. Scuseria, M. A. Robb, J. R. Cheeseman, J. A. Montgomery, Jr., T. Vreven, K. N. Kudin, J. C. Burant, J. M. Millam, S. S. Iyengar, J. Tomasi, V. Barone, B. Mennucci, M. Cossi, G. Scalmani, N. Rega, G. A. Petersson, H. Nakatsuji, M. Hada, M. Ehara, K. Toyota, R. Fukuda, J. Hasegawa, M. Ishida, T. Nakajima, Y. Honda, O. Kitao, H. Nakai, M. Klene, X. Li, J. E. Knox, H. P. Hratchian, J. B. Cross, V. Bakken, C. Adamo, J. Jaramillo, R. Gomperts, R. E. Stratmann, O. Yazyev, A. J. Austin, R. Cammi, C. Pomelli, J. W. Ochterski, P. Y. Ayala, K. Morokuma, G. A. Voth, P. Salvador, J. J. Dannenberg, V. G. Zakrzewski, S. Dapprich, A. D. Daniels, M. C. Strain, O. Farkas, D. K. Malick, A. D. Rabuck, K. Raghavachari, J. B. Foresman, J. V. Ortiz, Q. Cui, A. G. Baboul, S. Clifford, J. Cioslowski, B. B. Stefanov, G. Liu, A. Liashenko, P. Piskorz, I. Komaromi, R. L. Martin, D. J. Fox, T. Keith, M. A. Al-Laham, C. Y. Peng, A. Nanayakkara, M. Challacombe, P. M. W. Gill, B. Johnson, W. Chen, M. W. Wong, C. Gonzalez, and J. A. Pople, GAUSSIAN 03, Revision C.02, Gaussian, Inc., Wallingford, CT, 2004.
[33] T. H. Dunning, Jr., J. Chem. Phys. **90**, 1007 (1988).
[34] K. A. Peterson, B. C. Shepler, D. Figgen, and H. Stoll, J. Phys. Chem. A **110**, 13887 (2006).
[35] H.-J. Werner, P. J. Knowles, F. R. Manby, M. Schütz, P. Celani, G. Knizia, T. Korona, R. Lindh, A. Mitrushenkov, G. Rauhut, T. B. Adler, R. D. Amos, A. Bernhardsson, A. Berning, D. L. Cooper, M. J. O. Deegan, A. J. Dobbyn, F. Eckert, E. Goll, C. Hampel, A. Hesselmann, G. Hetzer, T. Hrenar, G. Jansen, C. Köppl, Y. Liu, A. W. Lloyd, R. A. Mata, A. J. May, S. J. McNicholas, W. Meyer, M. E. Mura, A. Nicklaß, P. Palmieri, K. Pflüger, R. Pitzer, M. Reiher, T. Shiozaki, H. Stoll, A. J. Stone, R. Tarroni, T. Thorsteinsson, M. Wang, and A. Wolf, MOLPRO, a package of *ab initio* programs, version 2008.1.
[36] G. N. A. van Veen, T. Baller, A. E. de Vries, and N. J. A. van Veen, Chem. Phys. **87**, 405 (1984).
[37] *NIST Chemistry WebBook*, NIST Standard Reference Database Number Vol. 69, edited by P. J. Linstrom and W. G. Mallard (National Institute of Standards and Technology, Gaithersburg MD, 2005), data retrieved from http://webbook.nist.gov, July 1, 2011.
[38] W. H. Pence, S. L. Baughcum, and S. R. Leone, J. Phys. Chem. **85**, 3844 (1981).
[39] A. B. Alekseyev, H.-P. Liebermann, and R. J. Buenker, J. Chem. Phys. **126**, 234103 (2007).
[40] T. A. A. Oliver, G. A. King, and M. N. R. Ashfold, Chem. Sci. **1**, 89 (2010).
[41] T. A. A. Oliver, G. A. King, and M. N. R. Ashfold, J. Chem. Phys. **133**, 194303 (2010).